White Rose Research Online

eprints@whiterose.ac.uk
https://eprints.whiterose.ac.uk
Universities of Leeds, Sheffield and York

Deposited via The University of Leeds.

White Rose Research Online URL for this paper:
https://eprints.whiterose.ac.uk/id/eprint/131329/

Version: Accepted Version

Article:
Gómez-Campos, FM, Rodríguez-Bolívar, S, Skibinsky-Gitlin, ES et al. (2018) Efficient, non-stochastic, Monte-Carlo-like-accurate method for the calculation of the temperature-dependent mobility in nanocrystal films. Nanoscale, 10 (20). pp. 9679-9690. ISSN: 2040-3364

https://doi.org/10.1039/c8nr00227d

© 2018, The Royal Society of Chemistry. This is an author produced version of a paper published in Nanoscale. Uploaded in accordance with the publisher's self-archiving policy.

Reuse
Items deposited in White Rose Research Online are protected by copyright, with all rights reserved unless indicated otherwise. They may be downloaded and/or printed for private study, or other acts as permitted by national copyright laws. The publisher or other rights holders may allow further reproduction and re-use of the full text version. This is indicated by the licence information on the White Rose Research Online record for the item.

Takedown
If you consider content in White Rose Research Online to be in breach of UK law, please notify us by emailing eprints@whiterose.ac.uk including the URL of the record and the reason for the withdrawal request.

Efficient, non-stochastic, Monte-Carlo-like-accurate method for the calculation of the temperature-dependent mobility in nanocrystal films†

Francisco M. Gómez-Campos,[a,b] Salvador Rodríguez-Bolívar,[a,b] Erik S. Skibinsky-Gitlin,[a] and Marco Califano,*[c]

We present a new non-stochastic framework for the calculation of the temperature dependence of the mobility in nanocrystal films, that enables speed-ups of several orders of magnitude compared to conventional Monte Carlo approaches, while maintaining a similar accuracy. Our model identifies a new contribution to the reduction of the mobility with increasing temperature in these systems (conventionally attributed to interactions with phonons), that alone is sufficient to explain the observed experimental trend up to room temperature. Comparison of our results with the theoretical predictions of the hopping model and the observed temperature dependence of recent field-effect mobility measurements in nanocrystal films, provides the means to discriminate between band-like and hopping transport and a definitive answer to whether the former has been achieved in quantum dot films.

Transport, mobility, nanocrystal films, colloidal quantum dot superlattices, pseudopotential method, temperature

1 Introduction

Continuing advances in synthetic methods yielding nearly monodisperse semiconductor nanocrystals, with uniform shape and composition[1,2], coupled with the ability to tailor the length of their capping agents (enabling interparticle separations from as small as 0.3 nm[2], down to virtually zero after annealing[3,5]), are paving the way to the creation of quantum dot superlattices with long-range order on the micrometre scale[1,2]. Such strongly coupled quantum dot films exhibit very high field-effect mobilities[5,6], whose observed increase with decreasing temperature has been interpreted as indication of band-like transport through extended states. However, as it was recently pointed out[7], a similar temperature dependence may also be exhibited by hopping transport, in a specific temperature range, and should therefore not be considered as incontrovertible evidence of band-like conduction. Indeed the mobility in the hopping regime is expected to depend on temperature exponentially, according to either $(1/T)\exp(-E_a/k_BT)$ (Einstein's relation)[7] or to $(1/\sqrt{T})\exp(-E_b/k_BT)$ (Marcus' theory)[8] (where E_a and E_b are some characteristic energies), whereas different expressions ($\mu \propto 1/T^x$ with x integer or fractional), derived from simple models, have been proposed for its temperature dependence in band-like transport[5,11]. An accurate theoretical determination of the temperature dependence of the mobility would provide the ability to discriminate between the two mechanisms at room temperature, where they may both exhibit a negative $d\mu/dT$, and a definitive answer to whether band-like transport has been achieved in quantum dot films.

This is what we aim to do here: We develop a new theoretical framework to calculate the temperature-dependent electron mobility in a semiconductor nanocrystal film (2D quantum dot superlattice), which approximates the accuracy of a full Monte Carlo calculation, at a much reduced computational cost. Our model combines an atomistic semiempirical pseudopotential approach[9], to obtain the wave functions for the isolated quantum dot, and a tight-binding formalism to solve the Schrödinger equation for the array[10]. Mobility is assumed to be limited by quantum dot size variations[11]. Starting from a suitably simplified Monte Carlo formulation of the problem, we derive expressions for the temperature-dependent electron mobilities in a quantum dot superlattice, which relate average velocities with the applied electric field. Our algorithm replaces the stochastic carrier flight times used in the Monte Carlo approach with their average. Their numerical fluctuations, unavoidable when using a finite sampling of the q-space, are then cleverly reduced by introducing a fractional occupancy function, based on accurate estimates for the miniband density of states. The use of Markov's chain framework further simplifies the description and the computational complexity of the whole dynamical process. Finally, the introduction of

[a] *Departamento de Electrónica y Tecnología de Computadores, Facultad de Ciencias, Universidad de Granada, 18071 Granada, Spain.*
[b] *CITIC-UGR, C/ Periodista Rafael Gómez Montero, n 2, Granada, Spain.*
[c] *Pollard Institute, School of Electronic and Electrical Engineering, University of Leeds, Leeds LS2 9JT, United Kingdom. E-mail: m.califano@leeds.ac.uk*

† Electronic Supplementary Information (ESI) available: [Smoothing procedure to remove fluctuations in the mobility caused by the finite discretization of the Q space]. See DOI: 10.1039/b000000x/

phonons allows the system to thermalize and provides a temperature dependence for the calculated mobility.

2 Theoretical method

Possible sources of scattering in nanocrystal films include structural disorder and interactions with phonons. According to a recently proposed theoretical expression for the mobility in quantum dot solids due to dark- and photo-conductivity[11], we assume that the former (fluctuations in the quantum dot sizes) represent the limiting mechanism for conduction. Phonon scattering is also present in the system, but its impact on the mobility is considered negligible[11], i.e.,

$$1/\mu_T = 1/\mu_{\text{phonons}} + 1/\mu_{\text{size variation}} \approx 1/\mu_{\text{size variation}} \qquad (1)$$

although its presence guarantees thermalisation. Indeed, despite recent findings[12] of a strong electron-phonon interaction in *bulk* polar semiconductors, electron-phonon coupling is expected to be strongly suppressed in 0D systems. In particular, in CdSe nanocrystals the Huang-Rhys parameter has been predicted[13–15] to be over 2 orders of magnitude smaller than in the bulk for both optical and acoustic modes.

Detailed expressions for phonon scattering rates in a quantum dot superlattice can be very difficult to obtain, because of the complex atomic distribution in the system. In our approach, however, such expressions are not required, as the interaction with phonons is captured through Fermi-Dirac's statistics, which the electron gas in the superlattice must obey because it is in thermodynamical equilibrium with the phonon's reservoir.

In a quantum dot superlattice under the drift effect of low electric fields (close to equilibrium conditions), in which size variation is the limiting mechanism for the mobility, the carrier stories include loops of series of a large number of slightly-drifted carrier flights, interrupted by energy-conserving (mobility-limiting) size variation scatterings, followed by temperature-dependent, energy-non-conserving (system-thermalising) phonon scattering events (in a negligible number compared to those due to the first mechanism). This scenario can be modelled using Monte Carlo simulations, which are ideally suited to study transport properties in semiconductors of any dimensionality[16–18]. Our approach, however, avoids the computationally expensive implementation of a full Monte Carlo algorithm by resorting to a non-stochastic simplification based on averaged quantities, which, nevertheless, allows it to retain the relevant physical description of the problem.

The miniband structure of the periodic system (Fig. 1) is obtained by solving the Schrödinger equation on a (51×51) grid discretization[19] of the Brillouin zone of the quantum dot superlattice within a tight-binding approach, where the wave functions of the periodic system are expanded in a basis of individual quantum dot conduction band eigenstates, obtained within the atomistic semiempirical pseudopotential framework[10]. Although we calculate up to 9 minibands (Fig. 1), the results presented here will focus on the mobility of the lowest energy miniband only.

The fact that size-variation scattering is an energy-conserving

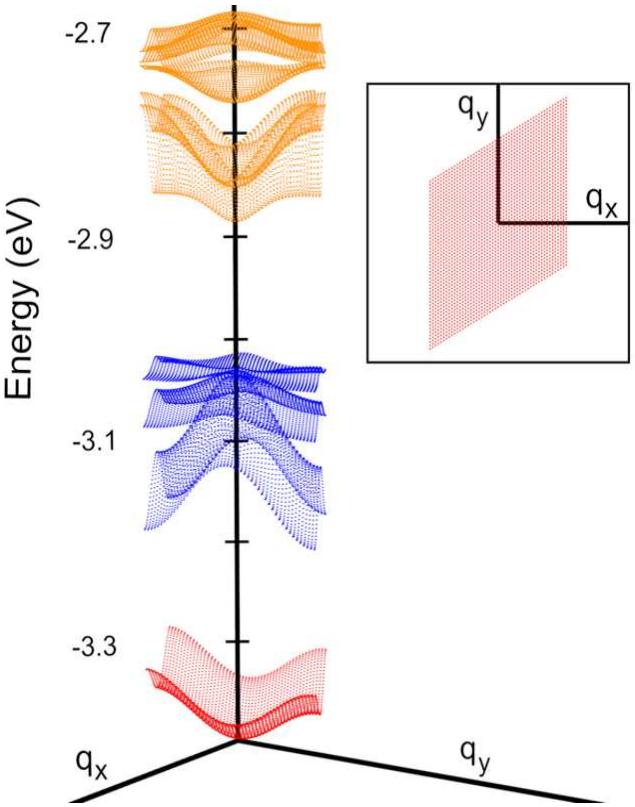

Fig. 1 Miniband structure for the lowest conduction band states in an hexagonal periodic structure of wurtzite CdSe quantum dots with radius 1.84 nm separated by a bond length. The inset shows the Brillouin zone in reciprocal space. The energies are referred to the vacuum level.

process implies that, within the miniband, there are sets of same-energy, mutually accessible states when only this mechanism is considered. In order to define such same-energy electron states we divided the miniband into a set of 100 equally-spaced energy intervals. With the typical miniband widths obtained in this study, the width of each resulting energy interval is about 1 meV. We assumed all the states within each energy interval to be mutually accessible after size-variation scattering events, and computed the respective mobility tensor (see below). In a second step the phonon thermalizing role was included by adding a weighting of the calculated mobility tensors by the thermal carrier population given by Fermi-Dirac's statistics, which finally led to a temperature-dependent expression for the mobility.

2.1 Mobility in an energy interval

The wave vector evolution $\vec{q}(t)$ is obtained from the set of miniband states in a particular energy interval using a semiclassical model:

$$\vec{q}(t) = \vec{q}_i - \frac{e}{\hbar}\vec{E}t \qquad (2)$$

where $\vec{q}_i$ is the initial wave vector, e is the absolute value of the electron charge, $\hbar$ is the reduced Planck constant, $\vec{E}$ is the applied electric field, and t is the flight time. In a Monte Carlo description, t would be a stochastic quantity that can be obtained from the scattering rates to the accessible states computed by Fermi's

Golden Rule. These size-variation scattering rates $\Gamma_{i\to f}$, from an initial state i to a final state f, are given by the following expression[10]:

$$\Gamma_{i\to f} = \frac{\gamma}{Q_{\rm st}}\frac{2\pi}{\hbar}\frac{1}{\Delta E}\frac{1}{\sqrt{K_{\vec{q}_i}K_{\vec{q}_f}}}\left|\sum_{m,s} b^*_{m,\vec{q}_f} b_{s,\vec{q}_i}\int \phi^*_m(\vec{r})\Delta V(\vec{r})\phi_s(\vec{r})d\vec{r}\right|^2 \tag{3}$$

where γ is the percentage of 'defect' (i.e., differently-sized) quantum dots in the superlattice, $Q_{\rm st}$ is the number of states in the Brillouin zone (51×51 in this study), ΔE is the width of the energy interval (~ 1 meV, here), $\phi_n(\vec{r})$ is the n-th wave function of the isolated quantum dot used in the tight-binding expansion for the periodic system (depending on their energy spread in our calculations we used from 9 to 11 single quantum dot wave functions), $b_{n,\vec{q}}$ is the coefficient multiplying the n-th state of the tight-binding expansion relative to a particular value for $\vec{q}$, $K_{\vec{q}}$ is the normalization constant of the periodic system wave function having wave vector $\vec{q}$, $\vec{q}_i$ and $\vec{q}_f$ are the wave vectors before (i) and after (f) the scattering, respectively, and $\Delta V(\vec{r})$ is the perturbation, i.e., the difference between the potentials of a 'normal-sized' quantum dot and a 'defect' quantum dot, which has an atomistic character in this study.

The new method presented in this paper (which is applicable to semiconductors of any dymensionality)[21], unlike Monte Carlo algorithms, assumes that the stochastic flight time can be substituted by the average flight time, which is the inverse of the summation of all the scattering probabilities to reach all the states in the same interval[21]. As a consequence:

$$\vec{q}_{{\rm fin},i} = \vec{q}_i - \frac{e}{\hbar}\vec{E}\frac{1}{\sum_f \Gamma_{i\to f}} \tag{4}$$

where $\vec{q}_{{\rm fin},i}$ is the final wave vector for the flight started from state q_i. The carrier velocity after the flight, $\vec{v}(\vec{q}_{{\rm fin},i})$, can be computed in a semiclassical fashion, i.e.

$$\vec{v}(\vec{q}_{{\rm fin},i}) = \frac{1}{\hbar}\nabla\varepsilon\Big|_{\vec{q}_{{\rm fin},i}}, \tag{5}$$

which involves the evaluation of the miniband energy gradient at $\vec{q}_{{\rm fin},i}$.

In a Monte Carlo description, each scattering process due to structural disorder has the probability

$$P_{i\to f} = \frac{\Gamma_{i\to f}}{\sum_{f'}\Gamma_{i\to f'}} \tag{6}$$

to take the system from an initial state i to a particular final state f within the same energy interval. Then a new flight starts with f as the initial state. This procedure is repeated a large number of times, allowing the history of the carrier to be tracked within that specific energy interval, from which, in turn, the displacement, the average velocity and the mobility tensor can be obtained.

The present model tries to mimic the Monte Carlo method, using, however, a much more computationally efficient technique. Assuming the fractions $p_i = N_i/N_T$ to be known (where N_i is the number of flights starting from state i and N_T is the total number of flights simulated in a Monte Carlo calculation - usually a very large number), the carrier displacement within an energy interval can be estimated as

$$\vec{r} = \sum_{i=1}^{n_{\rm int}} \frac{p_i N_T \times \vec{v}(\vec{q}_{{\rm fin},i})}{\sum_f \Gamma_{i\to f}} \tag{7}$$

(where we implicitly assumed the drift to be a constant-velocity flight), and the total time of the simulation $t_{\rm sim}$ is simply the sum of all the flight times:

$$t_{\rm sim} = \sum_{i=1}^{n_{\rm int}} \frac{p_i N_T}{\sum_f \Gamma_{i\to f}}. \tag{8}$$

The average velocity can therefore be obtained by dividing (7) by (8)

$$\langle\vec{v}\rangle = \frac{\sum_{i=1}^{n_{\rm int}} \frac{p_i\times\vec{v}(\vec{q}_{{\rm fin},i})}{\sum_f\Gamma_{i\to f}}}{\sum_{i=1}^{n_{\rm int}}\frac{p_i}{\sum_f\Gamma_{i\to f}}} \tag{9}$$

Our model differentiates itself from the cumbersome Monte Carlo approach by resorting to Markov's theory formalism[20] for the computation of the unknown fractions p_i. Indeed, the scattering process considered here is an example of Markov chain[20]. The $n_{\rm int}\times n_{\rm int}$ transition probability matrix between all states is constructed starting from the known $P_{i\to f}$ (6).

In the spirit of Markov's formalism we calculated the 10^4th power of such a matrix (equivalent to computing the probability after 10^4 transitions) obtaining the probabilities p_i of starting flights from each of the $n_{\rm int}$ states. The result of this procedure is that, after such a large number of transitions, all the matrix's columns are the same, so that the memory of the state from which the first flight started is lost, and the probability is independent of the initial state. This enables a 4-orders-of-magnitude speedup compared to conventional Monte Carlo methods, making it possible to run a full calculation in less than 12 hours on a single CPU, and a considerable improvement in the dispersion of our results (which is reduced by a factor of $1/\sqrt{N}$, where N is the number of scattering events).

For a given applied field, the mobility could then be obtained from $\langle\vec{v}\rangle = \hat{\mu}\vec{E}$. However, in order to obtain the four components of the mobility tensor $\hat{\mu}$ in the planar periodic system for any particular energy interval in the miniband, two separate calculations are needed, each with the electric field pointing along a different direction.

As the negative charge of the electron causes the velocity to be opposite to the applied electric field, the mobilities should be negative. However, for the sake of clarity, and when indicated, we sometimes show their absolute value in the figures.

2.2 Total mobility

The total mobility tensor is obtained as a combination of the mobility tensors $\hat{\mu}_n$ calculated for each energy interval n (containing $n_{{\rm int},n}$ states), weighted by the respective thermal population distribution $f_n(T,E_F)$

$$\hat{\mu}(T) = \frac{\sum_{n=1}^{100}\hat{\mu}_n f_n(T,E_F) n_{{\rm int},n}}{\sum_{n=1}^{100} f_n(T,E_F) n_{{\rm int},n}} \tag{10}$$

(the summation limit corresponds to the number of constant-energy intervals in which the miniband has been divided). As the tensor (10) is not necessarily diagonal, we present the eigenvalues μ_1 and μ_2 obtained by diagonalising it.

2.3 Sources of numerical noise

Before carrying out any calculation, however, it is necessary to determine a range of suitable values for the electric field, the dependence on which is contained in (5). Indeed, a value too low would drift the initial state to another state too similar to it, leading to numerical noise in the algorithm, whereas a value too high, apart from being inconsistent with the assumed conditions of near equilibrium for the system, would drift the initial state out of the energy interval to which it belongs. We performed a set of calculations for a 2D hexagonal periodic array of wurtzite CdSe quantum dots with radius 1.84 nm (the same system considered in section 3.A below), separated by a bond length, applying electric fields of different strengths along two perpendicular directions (x and y). The mobility tensor components calculated in three different energy intervals (1, 25 and 50) out of the set of 100 considered are presented in Fig. 2. One should not try to associate a specific significance to the different components μ_{ij} separately: it is the result of the tensor diagonalization - the eigenvalues and eigenvectors - that is meaningful. The important point here is that this tensor should not depend on the applied field. The electric fields for which the different components are constant (10-1000 V/m) represent suitable values: we choose $E = 100$ V/m for all our calculations.

A further source of numerical noise in the results may be represented by our choice of Brillouin zone discretization (51×51), owing to the resulting different number of states in each interval. Such fluctuations could be reduced by reducing the number of intervals in which the miniband width is divided, but this strategy would lead to a relaxation of the energy conservation condition, and is therefore not a desirable solution. Another option could be to use a denser discretization of the reciprocal space, but this would result in an increased computational complexity, due to the increased number of transitions involved. The fluctuations are especially relevant in calculations at low temperatures when only the lowest energy intervals are populated and stem from the poor approximation for the actual density of states (i.e., that obtained with an infinitely dense discretization of the reciprocal space) obtained with our coarse sampling of the Brillouin zone. Taking into account the miniband 180 degree symmetry, the 51×51 discretization used here produces an even number of states in each interval which includes pairs of symmetrical q states (i.e., $\vec{q}$ and $-\vec{q}$, the exception being the lowest energy interval containing the Γ point $\vec{q} = 0$). This choice, while ensuring that the correct q states are assigned to each energy interval (i.e., that if $\vec{q}$ belongs to a particular interval, then $-\vec{q}$, which has the same energy, is also correctly included in the same interval), also leads to differences in the occupation numbers of neighbouring intervals which are multiples of 2. Such differences cause abrupt variations in the flight times calculated for these intervals, because in our model they depend on the occupation number of each interval (if, e.g.,

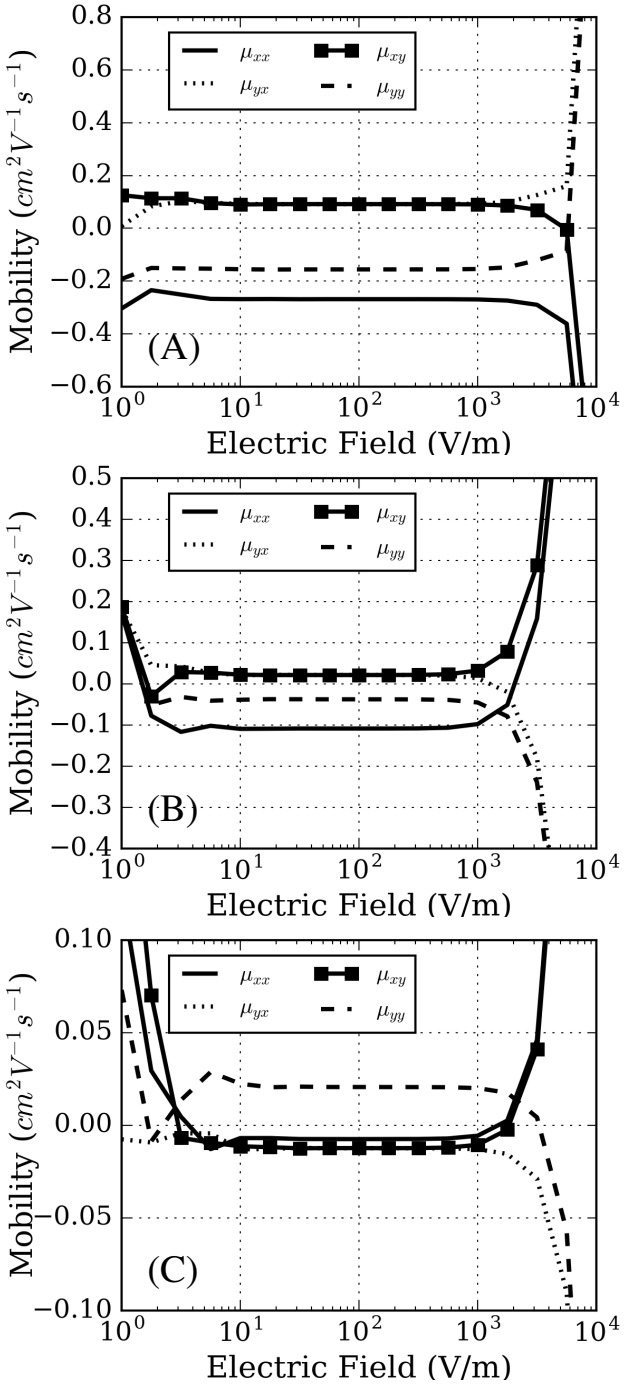

Fig. 2 Mobility tensor components calculated for the energy intervals 1 (-3.3955 eV with respect to the vacuum level, A), 25 (-3.3768 eV, B) and 50 (-3.3573 eV, C), as a function of the applied electric field.

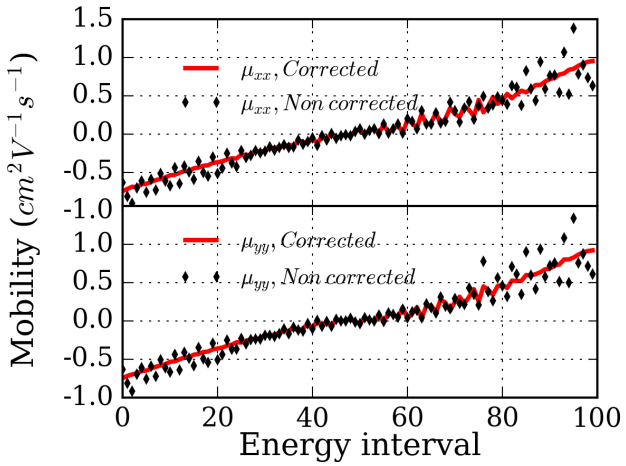

Fig. 3 Comparison between as-calculated (black symbols) and corrected (red line) mobility tensor components μ_{xx} and μ_{yy} for each energy interval in a square periodic structure of zincblende CdSe quantum dots with radius 1.84 nm separated by a bond length. Fluctuations are noticeably reduced when using fractional number of states in the energy intervals (see text).

interval i contains 10 states and interval $i+1$ contains 12 states, the 20% difference in their occupation numbers leads to a 20% difference in the respective flight times, which, in turn, yields a similar variation in the calculated mobilities). Furthermore, different discretizations may also yield noticeably different numbers of states in neighbouring intervals, leading to significant flight time fluctuations between them and, as a result, to considerable fluctuations in their mobilities. In order to correct for this effect we calculated the miniband structure by solving the Schrödinger equation for 500×500 q-points (instead of the 51×51 discretization in q-space used so far), obtaining the density of states in each of the 100 energy intervals. This more accurate estimate was then used to assign a fractional number of states to each energy interval of the 51×51 discretization[22], leading to low-fluctuation flight times (see Supporting Information)[†].

An example of this smoothing is shown in Fig. 3: The non-corrected mobility tensor components (black symbols) exhibit significant fluctuations in the highest energy intervals as well as in the three lowest ones, which are particularly relevant in the calculations at low temperature. The red curve shows how using fractional numbers of states derived from a 500 discretization corrects the flight times adequately and, as a consequence, removes most of the fluctuations from the calculated mobility tensor.

2.4 Influence of the Fermi level position

The position of the Fermi level also influences the mobility, through Fermi-Dirac's statistics (10). We investigated the effect of three different values for E_F: (i) at the minimum of the miniband, (ii) 100 meV below it, and (iii) 100 meV above it. The latter value was used just as test for the algorithm, because at that energy the additional effects of Pauli's exclusion principle need to be taken into account to obtain accurate mobility estimates.

The results are presented in Fig. 4(A): Both mobility eigenvalues increase with decreasing Fermi energies, for every value of

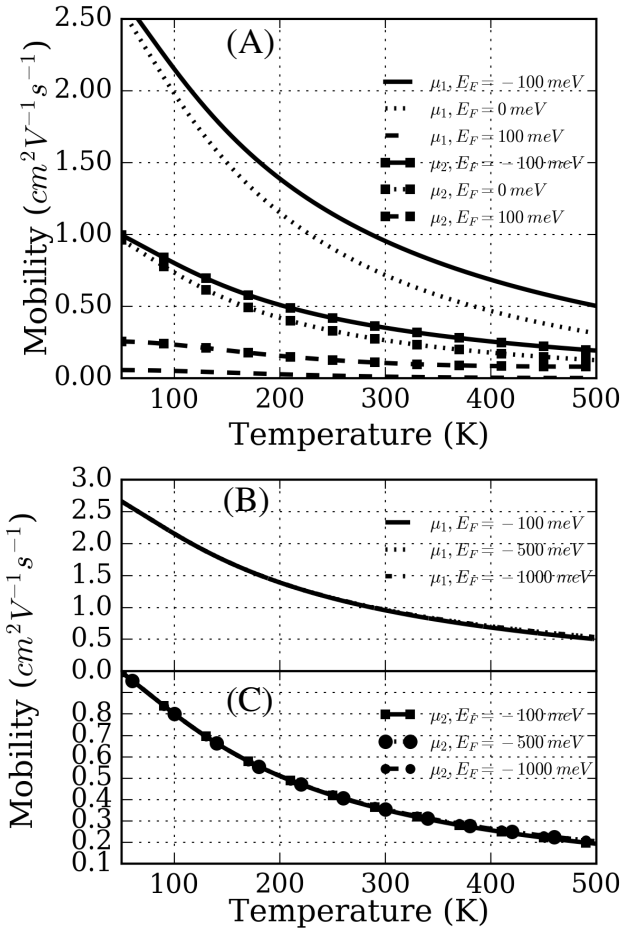

Fig. 4 Mobility eigenvalues vs temperature in an hexagonal periodic structure of wurtzite CdSe quantum dots with radius 1.84 nm separated by a bond length, calculated for different values of the Fermi energy level referred to the miniband minimum: $+100$ meV, 0 meV, -100 meV (A) and < -100 meV (B, C).

the temperature. We find, however, (Fig. 4(B)) that the mobilities become independent of the position of the Fermi level for $E_F < E_{\text{BandMin}} - 100$ meV. This result is not surprising considering that, for Fermi energies well below the miniband, Dirac's statistics in (10) becomes similar to Boltzmann's. In all the following calculations the Fermi level was therefore placed about 1.5 eV below E_{BandMin} (i.e., 5 eV below the vacuum level), in the CdSe bandgap.

3 Results and Discussion

3.1 Wurtzite CdSe dots with $R = 1.84$ nm

In this section we study the mobility dependence on temperature and dot-to-dot separation in 2D hexagonal periodic arrays of CdSe nanocrystals with $R = 1.84$ nm and a wurtzite crystal structure. The 'defect' quantum dots (i.e., the perturbations that originate the scattering process), represent the 1% of the total number of dots and have a radius of 1.7 nm (this corresponds to a size distribution of 7.6%). The calculations were performed for separations between centres of 3.68 nm, 3.77 nm, 3.87 nm and 3.95 nm, corresponding to wall-to-wall separations of 1 to

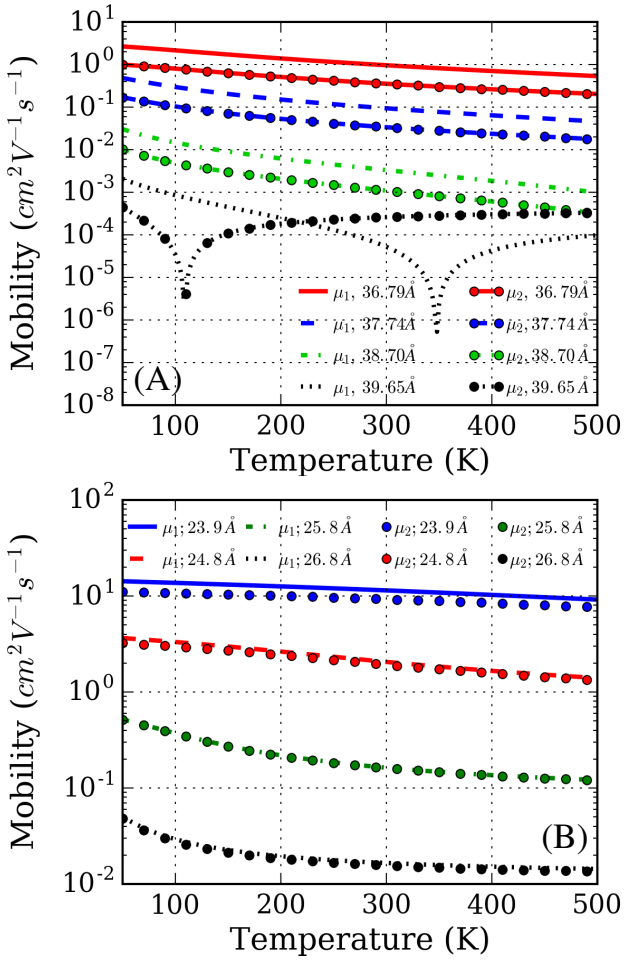

Fig. 5 Absolute value of mobility eigenvalues (μ_1 and μ_2) calculated for 2D hexagonal periodic arrangements of wurtzite CdSe nanocrystals with $R = 1.84$ nm (A) and $R = 1.26$ nm (B) with dot-to-dot separations from 1 to 2 bond lengths.

about 2 bond lengths[23] (0.26 to 0.52 nm), which are within a range achievable experimentally[5]. The results for the absolute value of the mobility eigenvalues, presented in Fig. 5(A), show a decreasing behaviour with increasing temperature and separation, in qualitative agreement with experiment[5,6]. The latter is found to be exponential and reflects the dependence exhibited by the calculated wave function overlaps (i.e., coupling) between neighbouring dots[24,25]: Increasing the separation by 3 Å reduces the mobility by three orders of magnitude. This large reduction is due to the fact that our model assumes the dots to be surrounded by vacuum. In a more realistic scenario, the presence of ligands would provide some coupling between the wave functions in neighbouring dots, mitigating the overlap reduction. We can therefore consider our results as a lower limit for the mobilities in these systems.

Interestingly both mobility eigenvalues exhibit a very different temperature dependence for a separation of 3.95 nm. We mentioned before that the mobility of the electron, due to the sign of its charge, should be negative. When the mobility changes sign and becomes positive, it must therefore relate to a positive charge carrier - the hole. We find that the mobility due to quantum dot size variations is electron-like around the miniband minimum and hole-like around the miniband maximum. At low temperatures the mobility is mainly determined by its behaviour at the miniband minimum. Increasing the temperature increases the contribution of higher energy intervals, leading, as a result, to a reduction of the total mobility. This constitutes an entirely new interpretation of the observed decrease in mobility with increasing temperature, conventionally attributed to carrier interactions with phonons, and here explained instead in terms of a purely energy-conserving mechanism. This reduction may eventually lead to a zero mobility, which means that hole-like transport balances electron-like transport. If hole-like transport dominates, the mobility changes sign and electrons in the miniband show hole-like mobility for the whole ensemble. This explains the observed behaviour around $T = 110$ K and 350 K for the largest quantum dot separation. At temperatures higher than 350 K [110 K] μ_1 [μ_2] is hole-like, and at lower temperatures electron-like, where it exhibits the same behaviour observed, in the whole range of temperatures, for all other quantum dot separations. The occurrence of this kind of behaviour makes it impossible to fit the mobility vs separation curves using a decreasing exponential function.

For smaller separations, we fitted the dependence on T of the absolute value of the mobility eigenvalues to the following expression:

$$\mu(T) = \frac{1}{(\alpha T + \beta)^n}. \tag{11}$$

The best fit ($R^2 = 0.9997$) was obtained for $n = 2$. The resulting values for α and β are shown in 1. As each simulation provides two mobility eigenvalues, two fitted values for both parameters are presented.

3.2 Wurtzite CdSe with $R = 1.26$ nm

We also studied electron transport when the 2D periodic structure is built from smaller quantum dots with $R = 1.26$ nm and the radius of the 'defect' dots (still representing 1% of the total) is 1.1 nm, corresponding to a size distribution of 10.4%(Fig. 5(B)). We find that, although, similarly to the previous case, increasing the quantum dot separation decreases mobility, the difference in the eigenvalues calculated for different separations is not as marked as for larger dots.

A more detailed inspection of our results reveals a higher anisotropy in the miniband structure obtained for larger nanocrystals than in that calculated for dots with $R = 1.2$ nm. This feature is evident in Fig. 6, where we show, for both systems, a cross section of the miniband taken 5 meV above the miniband minimum (here each dot represents a q state). Our results therefore indicate that the smaller the quantum dots, the more isotropic the minibands (which exhibit a similar curvature in every direction). Furthermore, the anisotropy around the miniband minimum exhibits maximum curvature along the diagonals of the Brillouin zone, i.e. along $\vec{b}_1 + \vec{b}_2$ and $\vec{b}_1 - \vec{b}_2$ (where $\vec{b}_1$ and $\vec{b}_2$ are the two-dimensional reciprocal space basis wave vectors). Therefore nearly-degenerate eigenvalues are obtained in arrays of smaller quantum dots. In contrast with the case of films of larger

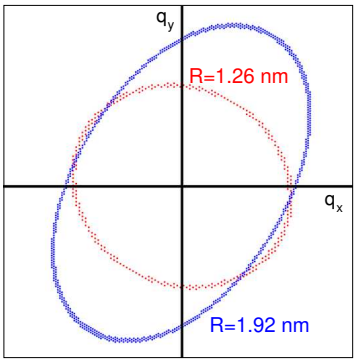

Fig. 6 States in reciprocal space located 5 meV above the miniband minima in 2D hexagonal periodic arrays of wurtzite CdSe nanocrystals with $R = 1.84$ nm (blue line) and $R = 1.26$ nm (red line).

dots, for small nanocrystal arrays we find no change in sign for the electron mobility in the temperature range considered. The results of the fitting of the mobility vs T curves to (11) (with $n = 2$)[26] are shown in 1. When the quantum dots are placed one bond length apart (the shortest separation considered here), we find that smaller quantum dots yield larger mobilities. In this case the highest mobilities are of the order of 10 cm^2/V·s.

3.3 Zincblende CdSe dots with $R = 1.22$ nm

In order to investigate the influence of the dot's crystal structure and the array's symmetry on the calculated mobilities, we considered zincblende CdSe nanocrystals in a square lattice. In this case the highest mobilities are found to be about one order of magnitude lower than for same-size wurtzite quantum dots in an hexagonal lattice (see Fig. 7A), mainly because of the lower coordination number of the array. For the largest dot-to-dot distance considered, the mobility eigenvalues show the change in sign already found for the larger wurtzite nanocrystals (Fig. 5), and no fitting was carried out consequently.

3.4 Cd-centred zincblende CdSe with $R = 1.22$ nm

In previous work[10] we found that the nanostructure's surface stoichiometry may have a considerable impact on the mobility in the 2D array. By growing the quantum dot around a central cation, instead of a Se atom (as it was the case for all structures considered so far), we obtained a Cd-rich surface. This choice reduces the mobility by a factor of up to about 2 (see Fig. 7B), for the shortest separations, and yields almost identical results to anion-centred structures for larger displacements. The atomic composition of the surface, therefore, seems to be important only for closely-spaced quantum dot arrays.

3.5 Dependence on the number of defects

All calculations so far have been carried out assuming the 'defect' dots to represent 1% of the total number of dots in the array. This value is not too far from present experimental capabilities[1], and well within the limits of applicability of our model[29,30], where we assume no correlations between defects. The effect of varying the defect ratio from 0.5% to 8%, is shown in Fig. 8. The dependence

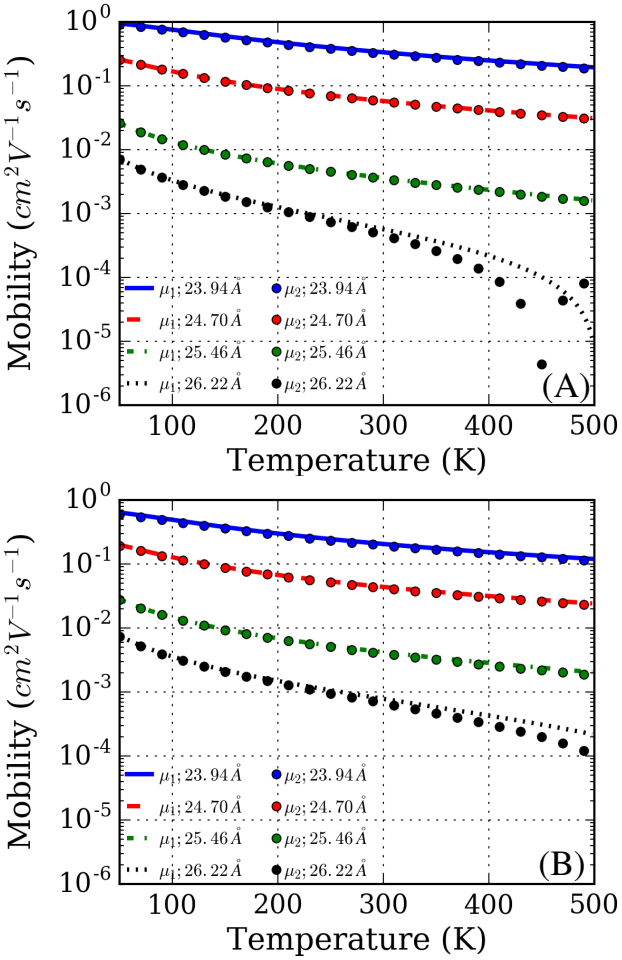

Fig. 7 Mobility eigenvalues ($|\mu_1|$ and $|\mu_2|$, in absolute value) for square periodic arrays of Se-centred (a) and Cd-centred (B) zincblende CdSe dots with $R = 1.2$ nm, calculated for different centre-to-centre separations: 2.39 nm (blue lines and symbols), 2.47 nm (red lines and symbols), 2.55 nm (green lines and symbols) and 2.62 nm (black lines and symbols).

on this ratio in our model is simplistic: an inspection of (3) reveals that the scattering probabilities are proportional to this quantity. This leads to flight times inversely proportional to the defect ratio.

3.6 Simplified ("Toy") model

Although it is not straightforward to see, we found that, in our treatment, the flight time dependence of the mobilities is the same as in the Drude model. Indeed, if we assume (i) the miniband to be parabolic with a specific effective mass and (ii) the transition rates $\Gamma_{i\to f}$ from every initial state to every final state to be equal in each interval, our approach will yield Drude's model. Our calculations show assumption (ii) to be reasonable (as an example, for a 2D hexagonal array of wurtzite CdSe nanocrystals with $R = 1.84$ nm, we find that the average over all the energy-conserving transitions in the miniband yields $\Gamma_{i\to f} = (1.3 \pm 0.04) \times 10^{14}$ s^{-1}). According to Markov's chain process, then the flight would have equal probability to start from any state in the interval. Furthermore, the flight times for all the states in the interval would be

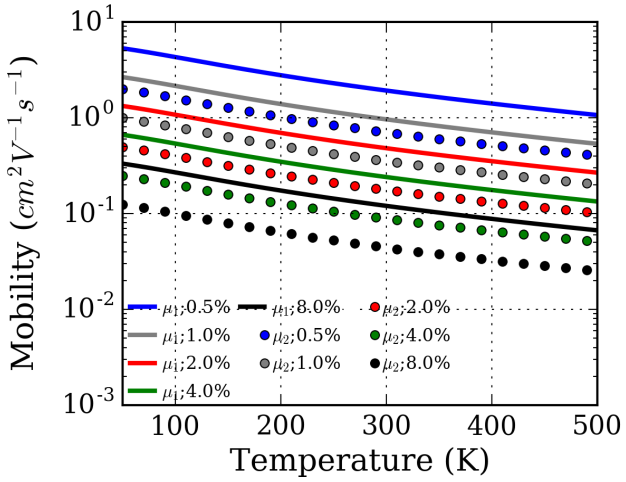

Fig. 8 Absolute value of the mobility eigenvalues vs temperature in hexagonal periodic arrays of wurtzite CdSe quantum dots with $R = 1.84$ nm and a 7.6% size dispersion, separated by a bond length, calculated for different defect ratios (0.5%, 1%, 2%, 4% and 8%).

equal too, because they are related to $\Gamma_{i\to f}$ by:

$$t_i = \frac{1}{\sum_f \Gamma_{i\to f}} \tag{12}$$

which, assuming a single rate $\tilde{\Gamma}$ for all transitions, simplifies to:

$$t_i = \frac{1}{\sum_f \Gamma_{i\to f}} \approx \frac{1}{n_{\text{int}}\tilde{\Gamma}}. \tag{13}$$

The transitions probabilities to each accessible final state after a scattering (6) would then become

$$P_{i\to f} = \frac{\Gamma_{i\to f}}{\sum_{f'} \Gamma_{i\to f'}} \approx \frac{1}{n_{\text{int}}} \tag{14}$$

(It needs to be stressed here that (12) to (14) refer to a *single* interval). These probabilities yield transition matrices for the Markov's chain that are themselves the limit matrix of the iterative process, and therefore no Markov's chain calculations are needed. The probabilities of starting a flight from a certain initial state i are then simply $p_i \approx 1/n_{\text{int}}$.

Once the group velocity along the miniband is calculated, the average velocity in an interval (9) could be simplified as:

$$\langle \vec{v} \rangle = \frac{\sum_{i=1}^{n_{\text{int}}} \frac{p_i \times \vec{v}(\vec{q}_{\text{fin},i})}{\sum_f \Gamma_{i\to f}}}{\sum_{i=1}^{n_{\text{int}}} \frac{p_i}{\sum_f \Gamma_{i\to f}}} \approx \frac{\sum_{i=1}^{n_{\text{int}}} \vec{v}(\vec{q}_{\text{fin},i})}{n_{\text{int}}}. \tag{15}$$

The value of $\vec{q}_{\text{fin},i}$ (4) can be obtained as:

$$\vec{q}_{\text{fin},i} \approx \vec{q}_{\text{ini}} - \frac{e}{\hbar\tilde{\Gamma} n_{\text{int}}}\vec{E} \tag{16}$$

and the mobility tensor in a given interval i in the presence of an electric field $\vec{E}$ is obtained as:

$$\hat{\mu}_i \approx \frac{1}{n_{\text{int}} \times E} \times$$
$$\begin{pmatrix} \sum_{i=1}^{n_{\text{int}}} v_x\left(q_{x,\text{ini}} - \frac{e}{\hbar\tilde{\Gamma} n_{\text{int}}}E, q_{y,\text{ini}}\right) & \sum_{i=1}^{n_{\text{int}}} v_x\left(q_{x,\text{ini}}, q_{y,\text{ini}} - \frac{e}{\hbar\tilde{\Gamma} n_{\text{int}}}E,\right) \\ \sum_{i=1}^{n_{\text{int}}} v_y\left(q_{x,\text{ini}} - \frac{e}{\hbar\tilde{\Gamma} n_{\text{int}}}E, q_{y,\text{ini}}\right) & \sum_{i=1}^{n_{\text{int}}} v_y\left(q_{x,\text{ini}}, q_{y,\text{ini}} - \frac{e}{\hbar\tilde{\Gamma} n_{\text{int}}}E,\right) \end{pmatrix} \tag{17}$$

Using this in (10) the mobility tensor's dependence on temperature is obtained.

When the miniband is isotropic and parabolic, and the calculation is carried out around its minimum, the dispersion relation can be written as:

$$\varepsilon(q_x, q_y) = \frac{\hbar^2}{2m}(q_x^2 + q_y^2) \tag{18}$$

The group velocity is then:

$$\vec{v} = \frac{1}{\hbar}\nabla\varepsilon(q_x, q_y) = \frac{\hbar}{m}(q_x, q_y) \tag{19}$$

The calculation of the mobility matrix terms, for example μ_{xx}, can be done by grouping together pairs of opposite initial $\vec{q}$ vectors in the interval, obtaining:

$$\mu_{xx} = \frac{\hbar}{m}\sum_{i=1}^{n_{\text{int}}/2} \frac{-2e}{\hbar\tilde{\Gamma} n_{\text{int}}}E = \frac{-e}{m\tilde{\Gamma}}E \tag{20}$$

which, finally, is Drude's mobility expression. (According to the latter, the mobility in each energy interval would be inversely proportional to the defect ratio, in agreement with our results).

The results of this simplified (or "Toy") model are compared with those of the full method in Fig. 10: the curves are indistinguishable. This proves that in each energy interval all the transition rates $\Gamma_{i\to f}$ can be considered equal ($\tilde{\Gamma}$). As a consequence $\tilde{\Gamma}$ can be extracted from a fit to experimental data. The results of this procedure are also shown in Fig. 10 where the best fits were obtained for the following values of $\tilde{\Gamma}$: 0.7×10^{13} s^{-1}, 10^{13} s^{-1}, and 1.2×10^{13} s^{-1}.

3.7 Dependence on dot-to-dot separation

Increasing the separation between dots reduces their mutual wave function overlap leading to a flattening of the minibands: The miniband effective mass increases and the mobility is reduced. The dependence of the overlap reduction with distance is approximately exponential, however, the complexities of the calculation and the influence of high-energy states far from the miniband minimum (especially at room and higher temperatures) could modify this exponential dependence. We investigated the effects of quantum dot separation at 50 K and 300 K (Fig. 9 - The centre-to-centre separations shown correspond to wall-to-wall separations of 1 to 2 bond lengths). At 50 K we expect to see the closest behaviour to an exponential decrease of mobility with displacement,

$$\mu_i(T, \Delta) = \gamma_i(T)e^{\eta(T)\Delta} \tag{21}$$

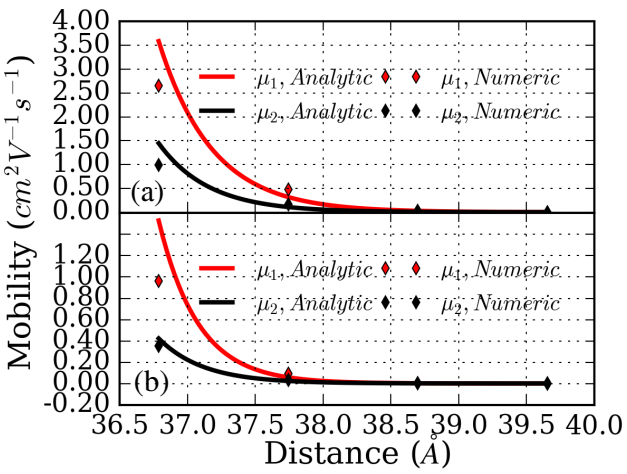

Fig. 9 Mobility eigenvalues (absolute values) vs quantum dot centre-to-centre distance in a hexagonal periodic array of wurtzite CdSe quantum dots with $R = 1.84$ nm, 7.6% size distribution, and 1% defect ratio (symbols) at $T = 50$ K (a) and $T = 300$ K (b). The analytical exponential fittings are shown as solid lines.

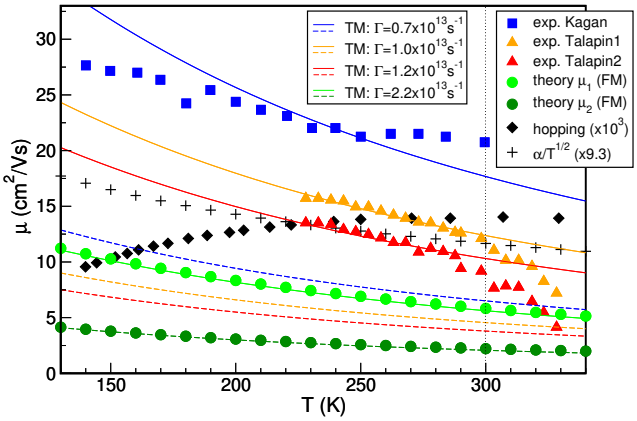

Fig. 10 The absolute values of the mobility eigenvalues as a function of temperature for wurtzite CdSe nanocrystals with $R = 1.84$ nm (1% defect density, 5% size distribution), calculated with our "Full Model" (FM) for wall-to-wall separations of 1 bond length (μ_1, full green circles; μ_2, full dark green circles), are compared with the theoretical predictions of (i) the hopping model obtained using the parameters suggested in Fig.2 of Ref.[7] and an activation energy $E_a = 25$ meV (black diamonds - values multiplied by 1000), and (ii) a recent model proposed by Shabaev and Efros[11] (where, for $E_F < E_{\text{BandMin}}$ (as we assume in our model) $\mu \propto 1/T^{1/2}$ - black crosses - values multiplied by 9.3), and with the experimental results reported by Talapin's group[6] for In_2Se_4-capped CdSe dots with $D = 3.9$ nm in both linear (orange triangles - Talapin1) and saturation (red triangles - Talapin2) regimes and the data from Kagan's group[5] relative to In-doped, thiocyanate-exchanged CdSe films made of similarly sized dots (blue squares). The solid and dashed lines represent the prediction of the "Toy Model" (TM) for μ_1 and μ_2 respectively, using the following values for Γ : 0.7×10^{13} s^{-1} (blue), 10^{13} s^{-1} (orange), 1.2×10^{13} s^{-1} (red), and 2.2×10^{13} s^{-1} (green). Shabaev and Efros' mobility curve is obtained according to Eq. (21) in Ref.[11], using our calculated values for overlap integrals and depth of the confining potential, and assuming a size dispersion of 5%. The curves relative to (i) the hopping model and (ii) Shabaev and Efros' model are rescaled (using multiplicative factors of 1000 and 9.3, respectively) so that they overlap with the red triangle at the lowermost temperature to allow for a fairer comparison of the different T dependencies.

(where $i = 1,2$ is the eigenvalue index, T is the temperature, $\Delta = d - d_0$, d is the wall-to-wall separation and $d_0 = 1$ bond length - the shortest distance considered here - both in Å), because at this temperature the main contribution to the calculation comes from the states around the miniband minimum, where the effective mass approach provides a suitable description of the system. Nevertheless, the mobilities still exhibit an exponential behaviour at 300 K, although the agreement with the exponential curves in Fig. 9 is not as good as for 50 K, due to the occurrence of instances where the mobility changes sign and the electron behaviour is hole-like. This occurs at high energies, when the miniband curvature is inverted.

The most interesting common feature for both eigenvalues is a larger decrease of mobility with separation at high temperatures than at low temperatures. The fitted exponential factors range between 1.9 and about 3.5, (see 2) with the exponent calculated at T=300 K about 20%-25% higher than that obtained at 50 K, roughly according to

$$\mu(300K, d-d_0) = \mu(300K, d_0) \times \left(\frac{\mu(50K, d-d_0)}{\mu(50K, d_0)} \right)^{5/4}. \quad (22)$$

As discussed earlier, we also find that smaller quantum dots show smaller reduction in mobility with increasing separation. This is due to a combination of two factors: (i) a stronger inter-dot coupling (i.e., a larger wave function overlap) and (ii) a more isotropic miniband for smaller quantum dots.

3.8 Comparison with hopping theory and experiment

Available experimental data for electron mobilities as a function of temperature have been measured, in a FET configuration, in $In_2Se_4^{2-}$-capped 3.9 nm CdSe nanocrystal arrays[6] and in In-doped, thiocyanate-exchanged CdSe films[5]. A direct quantitative comparison with these results is therefore difficult, as such systems are clearly very different from the ones studied here: (i) the nanocrystals are sandwiched between dielectric substrates and metal electrodes and (ii) their surface is covered by inorganic ligands that fill the inter-dot space. In contrast, we modelled an array with free surfaces whose constituents are separated by vacuum. Considering that the presence of inorganic ligands should increase the wave function overlap between neighbouring dots, compared to vacuum, and therefore increase electron mobilities, we expect our results to represent a lower limit for the mobilities measured in FETs. This expectation is confirmed by Fig. 10 which shows a comparison of our results for arrays of wurtzite CdSe nanocrystals with $R = 1.92$ nm, 1% defect ratio, 5% size dispersion, and an inter-dot separation of 1 bond length, with the measured field-effect experimental mobilities[5,6], and the predictions of the hopping model[7] (the curve displayed here was taken from Fig.2 of Ref.[7] and refers to $E_a = 25$ meV), and of a model recently proposed by Shabaev and Efros[11], where, for $E_F < E_{\text{BandMin}}$ (as we assume in our calculations), $\mu \propto T^{-1/2}$ (The curves relative to both hopping and Shabaev and Efros' models are rescaled (the former is multiplied by a factor of 1000 and the latter by a factor of 9.3) so that they overlap with the experimental data from Talapin's group (red triangles) at the lowermost

temperature, to allow for a fairer comparison of the different T dependencies). The experimental mobilities exhibit a very good qualitative and quantitative agreement with the temperature dependence predicted by band-like transport. Interestingly, they are fitted very well up to room temperature by the "Toy model" (TM) with $\tilde{\Gamma} = 0.7 - 1.2 \times 10^{13}$ s^{-1} (whereas the theoretical results of the "Full Model" (FM) are reproduced by the TM at all temperatures for $\tilde{\Gamma} = 2.2 \times 10^{13}$ s^{-1}). For higher temperatures, the observed mobilities show a steep drop from μ_1 to μ_2.

In contrast, the predictions of the hopping model[7]

$$\mu = \frac{\alpha E_a}{kT} e^{-E_a/kT} \tag{23}$$

(where α is a temperature-independent material- and configuration-specific parameter, E_a is the activation energy, k is Boltzmann's constant, and T the temperature), disagree with experiment both quantitatively (they are 3 orders of magnitude smaller), and, most importantly, qualitatively, as they exhibit the opposite trend with increasing temperature. While the quantitative disagreement could be mitigated by optimizing the choice of the exponential pre-factor α for the specific experimental samples considered, the prediction of an increase in the mobility with increasing temperature is a crucial feature that only depends on the value of the activation energy E_a (here $= 25$ meV). Smaller values for the activation energy would yield a better qualitative agreement with experiment (i.e., a negative slope for the curve), however they would be unrealistic, according to the estimated[7] magnitude of the different contributions to E_a (25 meV may already represent an underestimate for this quantity); whereas higher values for E_a increase the positive value for $d\mu/dT$ in this temperature range, hence the qualitative disagreement with experiment.

In contrast, the $\propto T^{-1/2}$ curve, although quantitatively about one order of magnitude smaller than the measured mobilities, is in better qualitative agreement with their observed T dependence, albeit in a restricted temperature range, if compared to our model. However, crucially, it cannot account for the observed drop in mobility above room temperature, which is instead captured in our approach by the second mobility eigenvalue μ_2.

4 Conclusions

We presented a new theoretical framework for the calculation of the temperature-dependent electron mobility in nanocrystal films, where fluctuations in the quantum dot sizes represent the limiting mechanism for conduction. Our approach is based on the Monte Carlo description of the scattering process in which, however, the stochastic carrier flight times are replaced by their average. This procedure avoids the computationally prohibitively expensive implementation of a full Monte Carlo algorithm while maintaining a similar accuracy. The use of Markov's chain formalism further improves the efficiency of the calculations, enabling speed-ups of over 4 orders of magnitude, compared to Monte Carlo.

The fluctuations in the flight times calculated in different isoenergetic intervals (due to the different number of states present in such intervals and unavoidable when using a finite discretization of the q space), which propagate to the mobilities causing similar variations, are substantially reduced by resorting to the definition of a smoothing function akin to the miniband density of states, further improving the accuracy of our results. Using this method, we investigated the effect on the electron mobility of dot size, dot-to-dot separation, density of defects, dot crystal structure and superlattice arrangement (square and hexagonal) for 2D arrays of CdSe nanocrystals.

Finally we validated the method by comparing its results with the experimental mobilities recently measured by two different groups. Our model shows that the observed mobility decrease with increasing temperature can be explained up to room temperature without resorting to phonon scattering, but in terms of the hole-like character of the electron mobility at high energies. For higher temperatures, the phonons' contribution becomes dominant and causes the mobility to drop from its higher eigenvalue μ_1 to the lower eigenvalue μ_2. The comparison of the temperature dependence observed in the experimental field-effect mobilities and that predicted for hopping and band-like transport suggests the latter to be the mechanism at play in high mobility films.

Conflicts of interest

In accordance with our policy on Conflicts of interest There are no conflicts to declare.

Acknowledgements

M.C. gratefully acknowledges financial support from the School of Electronic & Electrical Engineering, University of Leeds. F.M.G.C. and S.R.B. were supported by Project ENE2016_80944_R, funded by the Spanish Ministerio de Economía, Industria y Competitividad.

Notes and references

1 Weidman, M. C.; Beck, M. E.; Hoffman, R. S.; Prins, F.; Tisdale, W. A. Monodisperse, Air-Stable PbS Nanocrystals via Precursor Stoichiometry Control. *ACS Nano* **2014**, *8*, 6363-6371.

2 Maulu, A.; Rodríguez Cantó, P. J.; Navarro Arenas, J.; Abargues, R.; Sanchez-Royo, J. F.; García Calzada, R.; Martínez-Pastor, J. P. Strongly-Coupled PbS QD Solids by Doctor Blading for IR Photodetection *RSC Adv.* **2016**, *6*, 80201-80212.

3 Baumgardner, W. J.; Whitham, K.; Hanrath, T. Confined-but-Connected Quantum Solids via Controlled Ligand Displacement *Nano Lett.* **2013**, *13*, 3225-3231.

4 Murray, C. B., Kagan, C. R. and Bawendi, M. G. Synthesis and Characterization of Monodisperse Nanocrystals and Close-Packed Nanocrystal Assemblies *Annu. Rev. Mater. Sci.* **2000**, *30*, 545-610.

5 Choi, J.-H.; Fafarman, A. T.; Oh, S. J.; Ko, D.-K.; Kim, D. K.; Diroll, B. T.; Muramoto, S.; Gillen, J. G.; Murray, C. B.; Kagan, C. R. Bandlike Transport in Strongly Coupled and Doped Quantum Dot Solids: A Route to High-Performance Thin-Film Electronics. *Nano Lett.* **2012**, *12*, 2631-2638.

6 Lee, J.-S.; Kovalenko, M. V.; Huang, J.; Chung, D. S.; Talapin, D. V. Band-like transport, high electron mobility and high

photoconductivity in all-inorganic nanocrystal arrays. *Nature Nanotechn.* **2011** *6*, 348-352.

7 Guyot-Sionnest, P. Electrical Transport in Colloidal Quantum Dot Films *J. Phys. Chem. Lett.* **2012**, *3*, 1169-1175.

8 Chu, I.-H.; Radulaski, M.; Vukmirovic, N.; Cheng, H.-P.; Wang, L.-W. Charge Transport in a Quantum Dot Supercrystal *J. Phys. Chem. C* **2011**, *115*, 21409-21415.

9 Wang, L.-W.; Zunger, A. Pseudopotential calculations of nanoscale CdSe quantum dots. *Phys. Rev. B* **1996**, *53*, 9579.

10 Gómez-Campos, F. M.; Rodríguez-Bolívar, S.; Califano, M. Mobility Toolkit for Quantum Dot Films *ACS Photon.* **2016**, *3*, 2059-2067.

11 Shabaev, A; Efros, Al. L; Efros, A. L. Dark and Photo-Conductivity in Ordered Array of Nanocrystals. *Nano Lett.* **2013**, *13*, 5454-5461.

12 Yang, J.-Y; Qin, G.; Hu, M. Nontrivial Contribution of Fröhlich Electron-Phonon Interaction to Lattice Thermal Conductivity of Wurtzite GaN. *Appl. Phys. Lett.* **2016**, *109*, 242103-1–242103-4.

13 Salvador, M. R.; Graham, M. W.; Scholes, G. D. Exciton-Phonon Coupling and Disorder in the Excited States of CdSe Colloidal Quantum Dots *J. Chem. Phys.* **2006**, *125*, 184709-

14 Nomura, S.; Kobayashi, T. Exciton-LO-Phonon Couplings in Spherical Semiconductor Microcrystallites *Phys. Rev. B* **1992**, *45*, 1305-1316.

15 Rodriguez-Suarez, R.; Menendez-Proupin, E.; Trallero-Giner, C.; Cardona, M. Multiphonon Resonant Raman Scattering in Nanocrystals *Phys. Rev. B* **2000**, *62*, 11006-11016.

16 R. E. Chandler, A. J. Houtepen, J. Nelson, and D. Vanmaekelbergh Electron Transport in Quantum Dot Solids: Monte Carlo Simulations of the Effects of Shell Filling, Coulomb Repulsions, and Site Disorder. *Phys. Rev. B* **2007**, *75*, 085325.

17 Gagorik, A. G.; Mohin, J. W.; Kowalewski, T.; Hutchison, G. R. Monte Carlo Simulations of Charge Transport in 2d Organic Photovoltaics *J. Phys. Chem. Lett.* **2013**, *4*, 36-42.

18 Ando, Y.; Cappy, A. Ensemble Monte Carlo Simulation for Electron Transport in Quantum Wire Structures *J. Appl. Phys.* **1993**, *74*, 3983-3992.

19 This choice produces an even number of states in each interval, which correctly include pairs of symmetrical q states (i.e., $\vec{q}$ and $-\vec{q}$, which have the same energy, the exception being the lowest energy interval containing the Γ point $\vec{q} = 0$), while, at the same time, ensuring reasonable/manageable computational times.

20 Basharin, G. P.; Langville, A. N.; Naumov, V. A. The Life and Work of A. A. Markov, *Linear Algebra and Its Application* **2004**, *386*, 3-26.

21 Jacoboni, C.; Reggiani, L. The Monte Carlo method for the solution of charge transport in semiconductors with applications to covalent materials, *Rev. Mod. Phys.* **1983**, *55* 645-705.

22 Unfortunately using the 500×500 discretization for the whole calculation is computationally too expensive.

23 Although the smallest centre-to-centre separation is equal to exactly $2R$, it nevertheless corresponds to a wall-to-wall separation of 1 bond length, as R is an "effective" radius, determined from the total number of atoms in the dot (N) as $R = a_0(3N/32\pi)^{1/3}$ (where a_0 is the material's lattice constant).

24 Yang, J.; Wise, F. W. Effects of Disorder on Electronic Properties of Nanocrystal Assemblies *J. Phys. Chem. C* **2015**, *119*, 3338-3347.

25 The exponential decrease of coupling with separation has also been confirmed experimentally[27,28].

26 In this case only, the curves relative to the greatest separation considered satisfy (11) with $n \sim 1/4$ instead.

27 Liu, Y.; Gibbs, M.; Puthussery, J.; Gaik, S.; Ihly, R.; Hillhouse, H. W.; Law, M. Dependence of Carrier Mobility on Nanocrystal Size and Ligand Length in PbSe Nanocrystal Solids *Nano Lett.* **2010**, *10*, 1960-1969.

28 Gao, Y.; Aerts, M.; Sandeep, C. S. S.; Talgorn, E.; Savenije, T. J.; Kinge, S.; Siebbeles, L. D. a; Houtepen, A. J. Photoconductivity of PbSe Quantum-Dot Solids: Dependence on Ligand Anchor Group and Length *ACS Nano* **2012**, *6*, 9606-9614.

29 Rodríguez-Bolívar, S.; Gómez-Campos, F. M.; Luque-Rodríguez, A.; López-Villanueva, J. A.; Jiménez-Tejada, J. A.; Carceller, J. E. Miniband structure and photon absorption in regimented quantum dot systems *J. Appl. Phys.* **2011**, *109*, 074303-1 - 074303-7.

30 García, T.; Gómez-Campos, F. M.; Rodríguez-Bolívar, S. Influence on miniband structure of size variations in regimented InAs/GaAs quantum dots arrays. *J. Appl. Phys.* **2013**, *114*, 064311-1 - 064311-6.

Table 1 Fitted parameters from (11) with $n = 2$. The subscripts refer to each of the mobility eigenvalues μ_1 and μ_2

R[nm]	Cr. Struct.	Surface	d [nm]	$\alpha_1[\sqrt{Vs}/\mathrm{cmK}]$	$\alpha_2[\sqrt{Vs}/\mathrm{cmK}]$	$\beta_1[\sqrt{Vs}/\mathrm{cm}]$	$\beta_2[\sqrt{Vs}/\mathrm{cm}]$
1.84	WZ	Se-rich	3.7	5.38×10^{-4}	8.72×10^{-4}	1.61	2.68
1.84	WZ	Se-rich	3.8	2.23×10^{-3}	3.54×10^{-3}	3.62	6.44
1.84	WZ	Se-rich	3.9	1.70×10^{-2}	3.00×10^{-2}	6.97	11.17
1.26	WZ	Se-rich	2.4	4.36×10^{-5}	4.58×10^{-5}	0.91	0.80
1.26	WZ	Se-rich	2.5	2.39×10^{-4}	2.31×10^{-4}	1.49	1.59
1.26	WZ	Se-rich	2.6	1.04×10^{-3}	1.04×10^{-3}	4.43	4.46
1.22	ZB	Se-rich	2.4	8.89×10^{-4}	9.13×10^{-4}	2.77	2.83
1.22	ZB	Se-rich	2.5	2.58×10^{-3}	2.61×10^{-3}	5.27	5.27
1.22	ZB	Se-rich	2.6	1.27×10^{-2}	1.32×10^{-2}	14.67	14.17
1.22	ZB	Cd-rich	2.4	1.17×10^{-3}	1.21×10^{-3}	3.41	3.48
1.22	ZB	Cd-rich	2.5	3.03×10^{-3}	2.92×10^{-3}	6.12	6.14
1.22	ZB	Cd-rich	2.6	1.10×10^{-2}	1.18×10^{-2}	15.38	14.56

Table 2 Fitted parameters from (21). The subscripts refer to each of the mobility eigenvalues μ_1 and μ_2.

R[nm]	Cr. Struct.	Surface	T [K]	$\gamma_1[\mathrm{cm}^2/\mathrm{Vs}]$	$\gamma_2[\mathrm{cm}^2/\mathrm{Vs}]$	$\eta_1[\mathrm{\AA}^{-1}]$	$\eta_2[\mathrm{\AA}^{-1}]$
1.84	WZ	Se-rich	50	1.45	3.59	-2.712	-2.537
1.84	WZ	Se-rich	300	1.53	0.42	-3.433	-3.024
1.26	WZ	Se-rich	50	17.41	14.16	-1.952	-1.880
1.26	WZ	Se-rich	300	13.05	11.13	-2.287	-2.236
1.22	ZB	Se-rich	50	1.04	1.01	-2.228	-2.218
1.22	ZB	Se-rich	300	0.38	0.38	-2.883	-2.949
1.22	ZB	Cd-rich	50	0.71	0.68	-2.008	-1.990
1.22	ZB	Cd-rich	300	0.23	0.22	-2.508	-2.553